ExoMol line lists – XLVII. Rovibronic spectrum of aluminium monochloride (AlCl)

Sergei N. Yurchenko[1]★, Emma Nogué[1,2], Ala'a A.A. Azzam[3,4] and Jonathan Tennyson[1]†

[1] *Department of Physics and Astronomy, University College London, Gower Street, WC1E 6BT London, UK*
[2] *Department of Physics, Université Toulouse III - Paul Sabatier, Toulouse, France*
[3] *Department of Physics, The University of Jordan, Queen Rania Street, Amman 11942, Jordan*
[4] *AstroJo Institute, Amman, Jordan*

Accepted XXXX. Received XXXX; in original form XXXX

ABSTRACT

A line list for two isotopologues of aluminium monochloride, $AlCl^{35}$ and $AlCl^{37}$ are presented covering the wavelength range $< 0.2\,\mu$m, J up to 400 and applicable for temperatures up to 5000 K. The line lists are built using an empirical spectroscopic model consisting of potential energy curves, spin-orbit coupling curves, electronic angular momentum curves and Born-Oppenheimer Breakdown correction curves combined with *ab initio* dipole moments and covers the four lowest electronic states, $X\,^1\Sigma^+$, $A\,^1\Pi$, $a\,^3\Pi$ and $b\,^3\Sigma^+$. Considerable problems with the assignments of some the laboratory rovibronic spectra are identified. Treatment of the states lying in the continuum is discussed. The YNAT line list is available from the ExoMol database at www.exomol.com.

Key words: molecular data – opacity – planets and satellites: atmospheres – stars: atmospheres – ISM: molecules.

1 INTRODUCTION

The aluminium monochloride (AlCl) molecule is a well-known species in the envelope of the carbon star IRC+10216 (Cernicharo & Guelin 1987; Agundez et al. 2012). AlCl has also been detected in circumstellar envelope of the red AGB stars R Dor and IK Tau (Decin et al. 2017) and recently in an S-type AGB star W Aquilae Danilovich et al. (2021). The GChen model calculations of Woitke et al. (2018) predict that AlCl should be prominent in the atmospheres of hot exoplanets but its detection has so far been inhibited by the absence of a line list covering shorter wavelengths (Chubb et al. 2020).

There are many experimental studies of AlCl spectra (Sharma 1951; Reddy & Rao 1957; Hedderich et al. 1993; Hensel et al. 1993; Hoeft et al. 1973; Kumar et al. 1985; Lide 1965; Wyse & Gordy 1972; Ram et al. 1979, 1982; Saksena et al. 1998; Welz et al. 2006; Mahieu et al. 1989a,b; Daniel et al. 2021), see also the summary by Welz et al. (2006). Recent interest in AlCl has been sparked by the proposal that is an excellent candidate for laser cooling (Daniel et al. 2021).

An empirical AlCl line list was provided by Yousefi & Bernath (2018) and made available as part of the ExoMol database (Wang et al. 2020). However, this line list only considers transitions within the ground $X\,^1\Sigma^+$ state ($v = 0$ to $v = 11$ and up to $J_{\max} = 200$). There have been a number of theoretical studies on the electronically excited states of AlCl, see Langhoff et al. (1988) and Xu et al. (2020) for example, but none of them provide line lists. However, *ab initio* temperature-dependent direct photodissociation cross sections and rates for AlCl were recently reported by Qin et al. (2021), based on multi-reference configuration interaction with a Davidson correction (MRCI+Q) calculations performed with an aug-cc-pV6Z basis set. Qin *et al.* reported MRCI potential energy curves (PECs) and transition dipole moments (TDMCs) for the singlet states of AlCl.

Here we construct line lists for both the main isotopologues, $Al^{35}Cl$ and $Al^{37}Cl$, which cover the four lowest electronic states, $X\,^1\Sigma^+$, $A\,^1\Pi$, $a\,^3\Pi$ and $b\,^3\Sigma^+$, as part of the ExoMol project (Tennyson & Yurchenko 2012). The line lists are constructed using an empirical spectroscopic model consisting of potential energy curves (PECs), spin-orbit curves (SOCs), electronic angular momentum curves (EMACs) and Born-Oppenheimer breakdown correction (BOB) curves curves of AlCl obtained by refining *ab initio* curves by fitting to experimentally derived energy values of $Al^{35}Cl$ and $Al^{37}Cl$. We use *ab initio* dipole moment curves (DMCs) and transition dipole moments curves (TDMs) computed as part of this work.

★ The corresponding author: s.yurchenko@ucl.ac.uk
† The corresponding author: j.tennyson@ucl.ac.uk

2 SPECTROSCOPIC MODEL

2.1 *Ab initio* calculations

To provide a starting point for construction of a spectroscopic model for the four-electronic-state system $X\,^1\Sigma^+$, $A\,^1\Pi$, $a\,^3\Pi$ and $b\,^3\Sigma^+$ of AlCL, we computed *ab initio* all relevant PECs, SOCs, EAMCs, DMCs and TDMCs at the MRCI+Q/aug-cc-pVQZ level of theory using program MOLPRO (Werner et al. 2012). The calculations used a (C_{2v} symmetry) active space of (11,4,4,1), internally-contracted state-averaging using 5, 4, 4, and 2 singlet states of symmetry $^1A_1$, $^1B_1$, $^1B_2$, $^1A_2$, respectively and 1,1,1 triplet states of symmetry $^3A_1$, $^3B_1$, $^3B_2$, respectively. All curves were computed on a dense grid of non-uniformly distributed 162 points, between r = 0.7 and 9.5 Å.

2.2 Analytical description

To represent the potential energy curves of the $X\,^1\Sigma^+$, $a\,^3\Pi$ and $b\,^3\Sigma^+$ states the following the extended Morse oscillator (EMO) function (Lee et al. 1999) was used:

$$V(r) = V_e \;+\; (A_e - V_e)\left[1 \;-\; \exp\left(-\sum_{k=0}^{N} B_k \xi_p^k (r - r_e)\right)\right]^2, \tag{1}$$

where A_e is a dissociation asymptote, $A_e - V_e$ is the dissociation energy, r_e is an equilibrium distance of the PEC, and ξ_p is the Šurkus variable given by:

$$\xi_p = \frac{r^p - r_e^p}{r^p + r_e^p}. \tag{2}$$

The corresponding expansion parameters were obtained by fitting to the empirical (MARVEL and pseudo-MARVEL) energies described below.

The shallow PEC of the $A\,^1\Pi$ state has a small barrier to the dissociation (see Fig. 1). We used a diabatic representation for this curve constructed from two PECs $V_1(r)$ and $V_2(r)$ coupled with a diabatic term $W(r)$ as a root of a characteristic 2×2 diabatic matrix

$$\mathbf{A} = \begin{pmatrix} V_1(r) & W(r) \\ W(r) & V_2(r) \end{pmatrix}. \tag{3}$$

The lower PEC $V_1(r)$ was taken as the EMO function in Eq. (1). The upper PEC $V_2(r)$ is a repulsive curve playing a role of a dummy state and represented using the following hyperbolic form (in cm^{-1} and Å):

$$V_2(r) = 42509.8 + \frac{310780.97}{r^6}, \tag{4}$$

with the asymptote fixed to the asymptote of the $A\,^1\Pi$ state, A_e = 42509.8 cm^{-1}. The coupling function $W(r)$ is given by

$$W(r) = \frac{1001.20}{\cosh[0.201(r - 2.668)]}, \tag{5}$$

where the parameters in Eqs. (4) and (5) are in cm^{-1} and Å. The upper curve and the coupling curve should be considered as effective objects fitted to create the appropriate shape of the $A\,^1\Pi$ PEC. The two eigenvalues of the matrix **A** are given by

$$V_{low}(r) \;\; = \frac{V_1(r) + V_2(r)}{2} - \frac{\sqrt{[V_1(r) - V_2(r)]^2 + 4\,W^2(r)}}{2}, \tag{6}$$

$$V_{upp}(r) \;\; = \frac{V_1(r) + V_2(r)}{2} + \frac{\sqrt{[V_1(r) - V_2(r)]^2 + 4\,W^2(r)}}{2}. \tag{7}$$

Only the lower component, V_{low}, is taken to represent the $A\,^1\Pi$ state and the other component, which is a dummy PEC, is disregarded in the rest of the calculations. In this decoupled way we could achieve a more stable fit.

In the refinement of the SOC and EAMC we use the *ab initio* curves, which are 'morphed' at the *ab initio* grid points using the following expansion:

$$F(r) = \sum_{k=0}^{N} B_k\, z^k (1 - \xi_p) + \xi_p\, B_\infty, \tag{8}$$

where z is either taken as the Šurkus variable $z = \xi_p$ or a damped-coordinate given by:

$$z = (r - r_{ref})\, e^{-\beta_2 (r - r_{ref})^2 - \beta_4 (r - r_{ref})^4}, \tag{9}$$

see also Prajapat et al. (2017) and Yurchenko et al. (2018). Here r_{ref} is a reference position equal to r_e by default and β_2 and β_4 are damping factors.

For the $X\,^1\Sigma^+$ state, a BOB correction curve modelled using Eq. (8) was used.

Intensities of the ground state overtone transitions are usually sensitive to the numerical noise and tend to form nonphysical plateau like structures for higher excitations. This can be partially improved using an analytical representation of the corresponding dipole moment curve as suggested by Medvedev et al. (2015). The electronic transitions do not seem to suffer from this effect. Here we used the double exponential

Table 1. Summary of $^{27}Al^{35}Cl$ experimental line positions used in the MARVEL analysis. The corresponding vibrational range is given in parentheses with each electronic state label, e.g. $X(8)$ from 72WyGo means that the $v_{max} = 8$ for state $X\,^1\Sigma^+$.

Reference	Tag	Range (cm^{-1})	States	N_{trans}
Lide (1965)	65Lide	0.972526 - 1.458736	X(1)	3
Wyse & Gordy (1972)	72WyGo	2.859968 - 9.231915	X(8)	69
Hensel et al. (1993)	93HeStJaMe	0.47482	X(0)	1
Hoeft et al. (1973)	73HoToTi	0.97254	X(0)	1
Daniel et al. (2021)	21DaWaRoHe	38198.8042 - 38240.9341	A(1)-X(1)	31
Hedderich et al. (1993)	93HeDuBe	0.486 - 511.465	A(8)-X(7)	1544
Saksena et al. (1998)	98SaDiSi	24541.6 - 24671.8	a(0)-X(0)	270

Table 2. Summary of $^{27}Al^{35}Cl$ experimental line positions used in the pseudo-MARVEL analysis. The corresponding range of vibrational states is given as parentheses with each electronic state label, e.g. $A(10)$ from 82RaRaUpRa means that the $v_{max} = 10$ for $A\,^1\Pi$.

Reference	Tag	States	Range (cm^{-1})	transitions
Ram et al. (1982)	82RaRuUpRa	$A(10) - X(14)$, $a(0) - X(0)$, $b(0) - a(2)$	17754.79 – 38425.9	2495
Mahieu et al. (1989a)	89MaDuBra	$A(10) - X(16)$	34489.261 – 39105.473	1938
Mahieu et al. (1989b)	89MaDuBrb	$b(0) - X(2)$	17764.412 – 24702.0173	1723

decay form in Eq. (8) to represent the DMC of the $X\,^1\Sigma^+$state. All parameters and grid values defining our spectroscopic model are provided in the supplementary material in the form of a Duo input file.

The curves representing our model are shown in Figs. 1 and 2.

2.3 MARVEL energy levels

The MARVEL (measured active rotation vibration energy levels) procedure (Furtenbacher et al. 2007; Császár & Furtenbacher 2011; Tóbiás et al. 2019) is a means of obtaining empirical energy levels by inverting high resolution laboratory spectra. We undertook a MARVEL analysis for $^{27}Al^{35}Cl$ for which there are a number of high resolution experimental studies available (Sharma 1951; Reddy & Rao 1957; Hedderich et al. 1993; Hensel et al. 1993; Hoeft et al. 1973; Kumar et al. 1985; Lide 1965; Wyse & Gordy 1972; Ram et al. 1979, 1982; Saksena et al. 1998; Welz et al. 2006; Mahieu et al. 1989a,b; Daniel et al. 2021). Some of these (Lide 1965; Wyse & Gordy 1972; Hoeft et al. 1973; Hedderich et al. 1993; Hensel et al. 1993; Daniel et al. 2021) also consider $^{27}Al^{37}Cl$ but the reduced amount of data available for this isotopologue was deemed insufficient to make a viable MARVEL network. Therefore for $^{27}Al^{37}Cl$ we simply use the infrared emission data of Hedderich et al. (1993) which we found to be reliable for both isotopologues. This allowed us to characterise the BOB effects in the electronic ground state.

Unfortunately not all the reports of $^{27}Al^{35}Cl$ spectra provided data useful for MARVEL. Reddy & Rao (1957) and Welz et al. (2006) contain no assignments, while we failed to obtain a copy of Ram et al. (1979). The assignments in a number of other sources (Ram et al. 1982; Mahieu et al. 1989a,b) provided to be inconsistent not only with other sources but even failed to obey combination differences within themselves. 98SaDiSi (Saksena et al. 1998) give reliable, but limited, data for the $a\,^3\Pi - X\,^1\Sigma^+$ band system. They suggest that 82RaRaUpRa (Ram et al. 1982) was misassigned and suggested an alternative assignment by shifting J values by 3. However, we found even with these new assignments 82RaRaUpRa still did not obey combination differences. Similarly Mahieu et al. (1989a,b) cover the $A\,^1\Pi - X\,^1\Sigma^+$ band system and their exclusion left us with the only rather limited (low J) coverage of the $A\,^1\Pi$ state provided by Daniel et al. (2021) plus the $a\,^3\Pi - X\,^1\Sigma^+$ data of (Saksena et al. 1998) to help characterise the electronically excited states. Given the need for even approximate data on the excited vibrational states of the electronic states of AlCl; use of these sources is discussed in the next subsection.

Table 1 presents a summary of the sources which we did include. The microwave studies due to Hoeft et al. (1973) and Hedderich et al. (1993) give hyperfine-resolved transitions; we simply averaged these transitions to provide the transitions with the same quantum numbers as the other sources. The quantum numbers used were electronic state label in pyvalem notation (eg X1Sigma+), total angular momentum (J), vibrational quantum number (v), fine structure counting number (F1,F2,F3) and total parity ($p = +/-$).

The sources we retained provide 1918 transitions for $Al^{35}Cl$ of which 1783 form a single network yielding 1079 energy levels. Interestingly, and somewhat unusually, for these sources all transitions were validated and therefore retained in our final runs. The input MARVEL transitions file and output MARVEL energy file are provided as part of the supplementary data.

According to Mahieu et al. (1989b), the $b\,^3\Sigma^+$ state should actually be of $^3\Delta$ symmetry, not $^3\Sigma^+$, which they claim is consistent with the *ab initio* calculations of Langhoff et al. (1988), although we did not find this in Langhoff *et al.* or, indeed, in subsequent electronic structure publications. This assumption also does not agree with Ram et al. (1982). We could not resolve the possible two Λ components structure of a $^3\Delta$ in our analysis. Our decision to treat b as $^3\Sigma^+$ appears to provide satisfactory results.

Table 2 gives a summary of the experimental data on $Al^{35}Cl$ not included in the MARVEL analysis due to their low resolution, large uncertainties or inconsistent assignment. We use this data in the next paragraph via a 'pseudo-MARVEL' procedure based on their combination differences.

Table 3. Example of combination differences for six $A\,^1\Pi - X\,^1\Sigma^+$ transitions from 89MaDuBra (Mahieu et al. 1989a), all of which reportedly connect to the same upper state $A\,^1\Pi$, $v' = 8$, $J' = 29$. The lower state energies are taken from the MARVEL set. The upper state energies are obtained using Eq. (10). The difference between the upper energies are significantly larger than the stated experimental uncertainty of 0.05 cm^{-1}.

ν cm^{-1}	J''	v''	E', cm^{-1}	E'', cm^{-1}
36361.099	28	11	41576.078	5214.979
35498.610	28	13	41575.242	6076.632
36770.410	30	10	41575.688	4805.278
36334.453	30	11	41576.055	5241.602
35901.836	30	12	41575.967	5674.131
35472.368	30	13	41575.270	6102.902

2.4 Pseudo-MARVEL energies

In the refinements an extended set of experimental energies of $Al^{35}Cl$ from Table 2 was constructed using ground state combination differences. The values were calculated as follows. First, the MARVEL energies described above were used as lower state energies $E_i^{(\mathrm{low})}$ in connection with the transition frequencies ν_{ij} of $Al^{35}Cl$ from the extended experimental set to to obtain the upper state energies $E_j^{(\mathrm{upp})}$

$$E_{j(i)}^{(\mathrm{upp})} = E_i^{(\mathrm{low})} + \nu_{ij}, \tag{10}$$

where the index (i) indicates the lower state i used. For the transitions to the same upper state j, this procedure allows us to obtain realistic estimates of the corresponding uncertainties of the experimental line positions. The upper state energy of the state j is then obtained by averaging $E_{j(i)}^{(\mathrm{upp})}$ over i:

$$E_j^{(\mathrm{upp})} = \overline{E_{j(i)}^{(\mathrm{upp})}} \pm \Delta E, \tag{11}$$

where ΔE is the corresponding estimated uncertainty of $E_j^{(\mathrm{upp})}$ from this averaging procedure. We call these $E_{j(i)}^{(\mathrm{upp})}$ pseudo-MARVEL energies. We found that many transitions from the extended experimental data in Table 2 exhibit uncertainties significantly larger than that claimed in the original publications. Table 3 shows an example of combination differences for six $A\,^1\Pi$–$X\,^1\Sigma^+$ transitions from Mahieu et al. (1989a) connecting the same upper state. The standard deviation for the estimated upper state energies is 0.4 cm^{-1} which is much higher than the uncertainty reported of 0.05 cm^{-1}. We set a threshold of 0.3 cm^{-1} and selected additional 910 pseudo-MARVEL energies to combine them with the pure MARVEL set of 1079 energies.

This procedure allowed us to significantly extend the vibrational coverage of the shallow $A\,^1\Pi$ state using the large sets of transitions provided by 89MaDuBra (Mahieu et al. 1989a) and 82RaRuUpRa (Ram et al. 1982), up to the last bound state $v = 10$. Vibrationally excited states play important role in refinements as they allow sampling larger ranges of r in the potential energy curves. Moreover, with this procedure we were also able to reconstruct the $v = 0$ rovibronic energies of the $b\,^3\Sigma^+$ state up to $J = 44$ using the transitions from 89MaDuBrb (Mahieu et al. 1989b) in conjunction with the $v = 0$ energies of $a\,^3\Pi$. These $b\,^3\Sigma^+$ $v = 0$ rovibronic states also appear as upper states in the larger experimental sets 82RaRuUpRa and 89MaDuBrb which connect them to a number of $a\,^3\Pi$ rovibronic states, not only with $v = 0$ (covered in the MARVEL data set), but also to the fundamental and overtone states of $v = 1, 2$, important for refining the shape of the PEC of $b\,^3\Sigma^+$. Using the pseudo-MARVEL energies of the vibronic state $v = 0$ $b\,^3\Sigma^+$ as upper states we could obtain $a\,^3\Pi$ $v = 1, 2$ pseudo-MARVEL energies via upper state combination differences as

$$E_{i(j)}^{(\mathrm{low})} = \overline{E_j^{(\mathrm{upp})} - \nu_{ij}}, \tag{12}$$

where the averaging is performed over the transitions corresponding to different upper states i connected to the same lower state j. As before, many of these combination differences suffered large uncertainties, so we applied the 0.3 cm^{-1} threshold and derived 411 additional pseudo-MARVEL term values for the $a\,^3\Pi$ state. The complete MARVEL + pseudo-MARVEL set of the $Al^{35}Cl$ energies is illustrated in Fig. 3.

2.5 Refinement

The model built from our *ab initio* PECs and couplings was refined using nuclear motion calculations performed with diatomic variational nuclear motion program Duo (Yurchenko et al. 2016). The rovibronic Schrödinger equation was solved for 4 coupled electronic states $X\,^1\Sigma^+$, $A\,^1\Pi$, $a\,^3\Pi$ and $b\,^3\Sigma^+$ using the methodology described in Yurchenko et al. (2016). The vibrational basis set was constructed by solving an uncoupled vibrational Schrödinger equations for each of the four electronic states using the Sinc DVR method on an equidistant grid of 500 radial points was used ranging from 0.7 to 4.0 Å and comprised 30, 20, 30 and 30 vibrational functions, respectively.

The $X\,^1\Sigma^+$ state MARVEL energies with high J have large experimental uncertainties and therefore were not strongly constrained in the fit, which is why the corresponding observed minus calculated (obs.-calc.) residuals increase at $J > 80$. All curves are given in the supplementary material as a Duo input file.

Using the experimentally derived energies of $Al^{35}Cl$, the PECs, SOCs and EAMCS were refined to build an empirical spectroscopic model

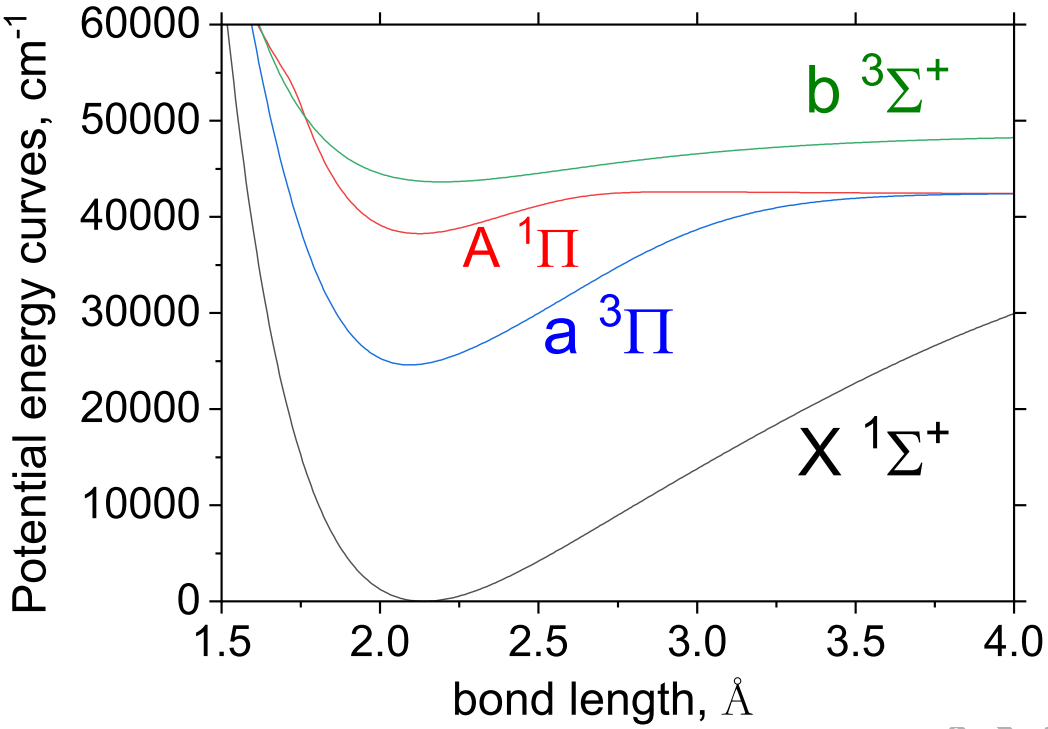

Figure 1. Refined potential energy curves of AlCl.

of $Al^{35}Cl$. The shallow $A\,^1\Pi$ state with a barrier contains bound vibrational states up to $v = 10$, all of which were included in the fit. The vibrational coverage of other states is also well represented, $v = 0 - 8$ for $X\,^1\Sigma^+$, $v = 0 - 2$ for $a\,^3\Pi$, while for the $b\,^3\Sigma^+$ state we only had $v = 0$ energies. The J excitations are up to $J = 100$, see Fig. 3.

The (adiabatic) $b\,^3\Sigma^+$ curve has a double well shape with a barrier at $r = 2.19$ Å. We could not reconstruct the full complexity of this curve and treated it using a simple one-well EMO-type PES, which effectively corresponds to the diabatic representation of this PEC. The obs.-calc. residuals of the calculated energy term values for the refined spectroscopic model are shown in Fig. 4.

For $Al^{37}Cl$, all the curves from the $Al^{35}Cl$ spectroscopic model, where the BOB of $X\,^1\Sigma^+$ was refined by fitting to the MARVEL energies of $Al^{37}Cl$ obtained from Hedderich et al. (1993). This improved the $X\,^1\Sigma^+$ state term values of $Al^{37}Cl$ to the quality of the $Al^{35}Cl$ isotopologue.

All curves representing our spectroscopic models for $Al^{35}Cl$ and $Al^{37}Cl$ are provided as part of the supplementary material to this paper in a form of a Duo input file.

2.6 Treating unbound states

The Duo methodology is developed for the bound-bound state problems with the effective boundary condition for the rovibronic eigenfunctions to vanish at the borders of the bond length grid. However our electronic system above the $A\,^1\Pi$ state dissociation includes region where unbound solutions are possible. Indeed a number of unbound eigenfunctions correspond to the unbound states with the exact zero at $r = r_{\rm max} = 4.0$ Å. For example, in our calculation the vibronic states of the shallow $A\,^1\Pi$ state are only bound for $v \leqslant 11$.

Although the Duo bound methodology can be applied to compute unbound, continuum spectra see Pezzella et al. (2021, 2022), in this work we are only interested in the bound spectrum. To the end, we first need to identify unbound wavefunctions $\psi_\lambda(r)$ and then exclude them from the line list production as follows. Unlike bound states, continuum wavefunctions do not vanish at large distances and can be identified by the non-zero density in the small region of δ =0.07 Å at the outer border $r_{\rm max}$:

$$\int_{r_{\rm max}-\delta}^{r_{\rm max}} |\psi_\lambda(r)|^2 dr > \epsilon \tag{13}$$

where we use $\epsilon = 10^{-8}$.

3 LINE LIST

Using the refined spectroscopic models and the dipole moment curves $X\,^1\Sigma^+$–$X\,^1\Sigma^+$, $X\,^1\Sigma^+$–$A\,^1\Pi$ and $b\,^3\Sigma^+$–$a\,^3\Pi$, we generated line lists for $Al^{35}Cl$ and $Al^{37}Cl$, containing bound states only (and transitions between them). We call these the YNAT line lists.

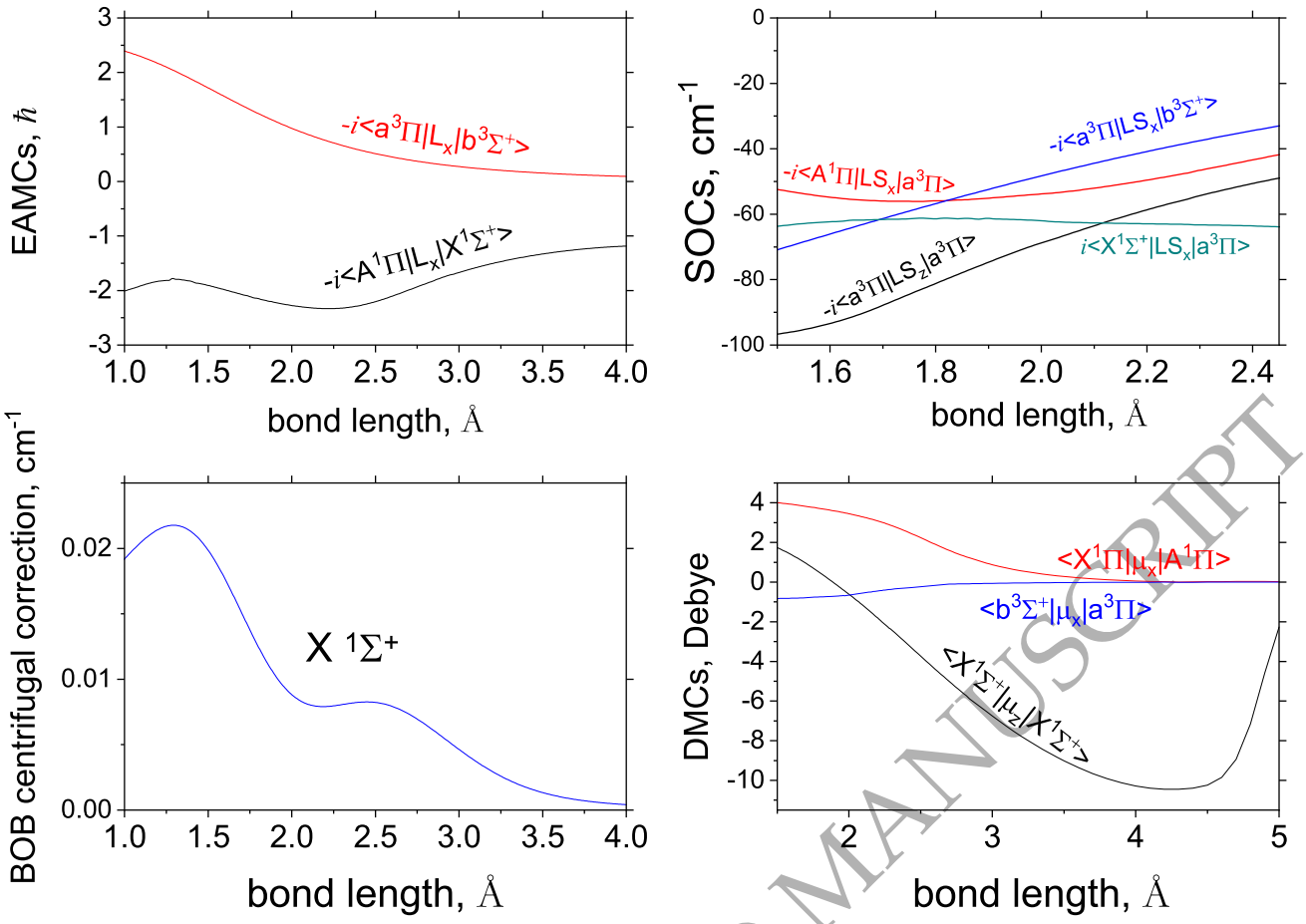

Figure 2. Refined EAMCs and Spin-Orbit curves, a BOB curve of X and *ab initio* (transition) dipole moments for AlCl.

The line list covers $J = 0 \ldots 400$ withwavenumbers from 0 to 50000 cm^{-1}, including the $b\,^3\Sigma^+$-$a\,^3\Pi$ band region. Each line list is built from two files, States and Transition. They have standard ExoMol format (Tennyson et al. 2013, 2020) with the standard set of quantum numbers as generated by Duo and have been extensively described elsewhere (see e.g. Yurchenko et al. (2022)). Extracts from the line list files, States and Trans, are given in Tables 4 and 5.

Partition functions for Al^{35}Cl and Al^{37}Cl were generated by summing over the (MARVELised) energy levels of the YNAT line lists which extend up to $J = 400$. This should be sufficient to converge the partition sum up to $T = 5000$ K. Figure 5 compares our results with the more approximate compilation due to Barklem & Collet (2016). As we follow the HITRAN convention (Gamache et al. 2017) and use the full nuclear-spin degeneracy, it is necessary to scale Barklem and Collet's values. Both ^{35}Cl and ^{37}Cl have nuclear spin $I = \frac{3}{2}$ while ^{27}Al has $I = \frac{5}{2}$ which gives multiplicative factor of $(2I_{\rm Cl} + 1) \times (2I_{\rm Al} + 1) = 4 \times 6 = 24$ for both Al^{35}Cl and Al^{37}Cl. With this scaling we find satisfactory agreement between the partition sums for temperatures of importance. Our partition functions for Al^{35}Cl and Al^{37}Cl are given in the supplementary data.

4 SPECTRA

Figure 6 shows an overview of the Al^{35}Cl spectrum up to 50000 cm^{-1} for temperature of $T = 2000$ K. Besides transitions within the $X\,^1\Sigma^+$ ground state, the most prominent feature is the extended $A\,^1\Pi - X\,^1\Sigma^+$ band system which peaks in the blue. The forbidden bands $b\,^3\Sigma^+$-$X\,^1\Sigma^+$ and $a\,^3\Pi$-$X\,^1\Sigma^+$ originate from the coupling of the corresponding states by stealing intensities from the allowed bands.

Figure 7 compares the emission spectrum by Hedderich et al. (1993) to our simulations, showing a satisfactory agreement.

On Earth the abundance ratio of ^{35}Cl to ^{37}Cl is close to 3:1. Figure 8 gives two illustrative spectra of AlCl assuming a terrestrial isotope ratio.

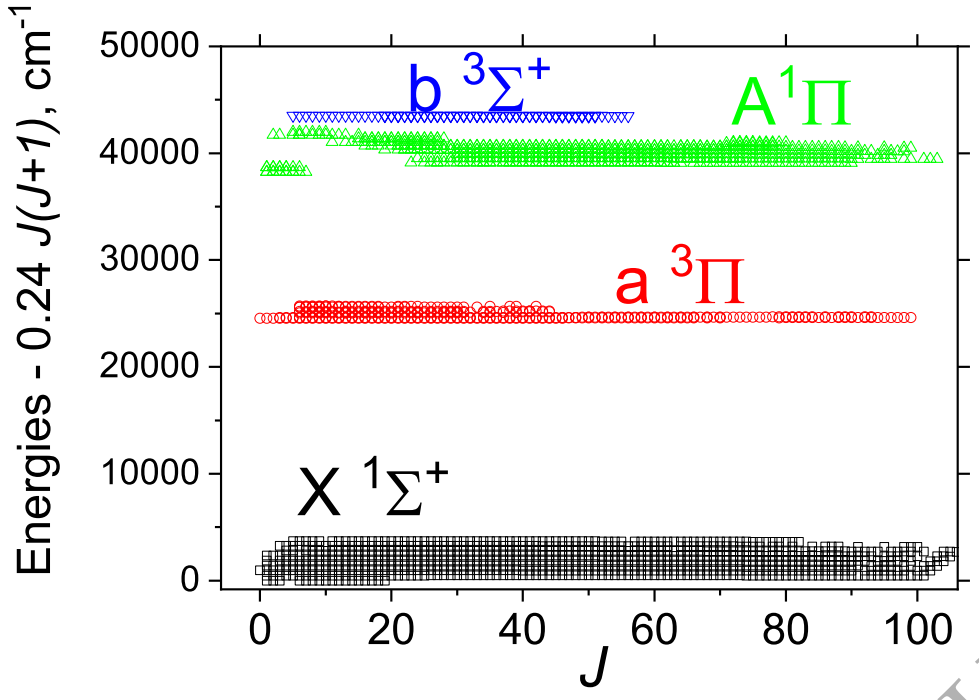

Figure 3. Illustration of the experimentally derived energy term values used of $Al^{35}Cl$ in the refinement of the *ab initio* spectroscopic model.

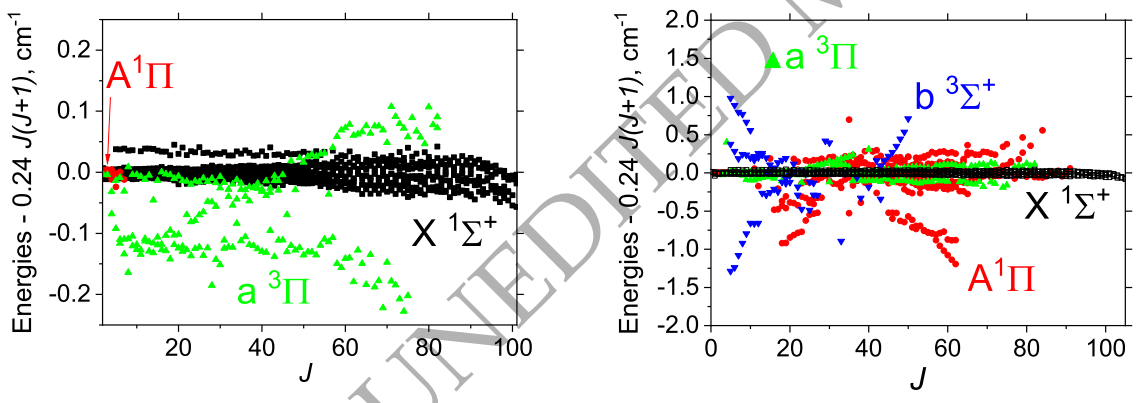

Figure 4. $Al^{35}Cl$ obs.-calc. residuals of the refined spectroscopic model. Left: For the MARVEL energies only; Right: all energies including pseudo-MARVEL.

5 CONCLUSIONS

Rovibronic line lists for two main isotopologues of AlCl are presented. These line list, called YNAT, cover both pure bound-bound transitions and bound-quasibound features lying in the continuum; they are available from `www.exomol.com` (Tennyson et al. 2020) and from `www.zenodo.org` (European Organization For Nuclear Research & OpenAIRE 2013). The importance for astronomical studies of correctly treating the lifetime broadening which are a feature of quasibound spectra has recently been highlighted by Yurchenko et al. (2022). We plan to extend our treatment of such spectra to correctly allow for this in future work.

Although there have been a number of high resolution studies of studies of the spectrum of AlCl we found serious problems with a studies spanning many of the electronic excited states of this system. More experimental work on this problem would be welcome and would help improve the list lists.

Table 4. Extract from the states file of the line list for $Al^{35}Cl$.

i	Energy (cm^{-1})	g_i	J	unc	Parity	State	v	Λ	Σ	Ω
517	37115.05983	120	2	0.8	+ e	a3Pi	28	1	-1	0
518	37369.53092	120	2	0.8	+ e	a3Pi	29	1	1	2
519	37421.68121	120	2	0.8	+ e	a3Pi	29	1	0	1
520	37473.97733	120	2	0.8	+ e	a3Pi	29	1	-1	0
521	38238.93188	120	2	0.8	+ e	A1Pi	0	1	0	1
522	38680.24603	120	2	0.8	+ e	A1Pi	1	1	0	1
523	39109.98831	120	2	0.8	+ e	A1Pi	2	1	0	1
524	39527.24815	120	2	0.8	+ e	A1Pi	3	1	0	1

i: State counting number.
$\tilde{E}$: State energy term values in cm^{-1}, MARVEL or Calculated (Duo).
g_i: Total statistical weight, equal to $g_{ns}(2J+1)$.
J: Total angular momentum.
unc: Uncertainty, cm^{-1}.
+/−: Total parity.
State: Electronic state.
v: State vibrational quantum number.
Λ: Projection of the electronic angular momentum.
Σ: Projection of the electronic spin.
Ω: Projection of the total angular momentum, $\Omega = \Lambda + \Sigma$.

Table 5. Extract from the transitions file of the line list for $Al^{35}Cl$.

f	i	A_{fi} (s^{-1})	$\tilde{\nu}_{fi}$
11176	10659	8.4054E-07	1000.000993
26971	26795	1.3906E-06	1000.008628
6040	6203	1.2663E-05	1000.011118
27111	26595	1.5160E-08	1000.011830
10789	10273	4.3846E-07	1000.014773
10649	10473	3.6054E-07	1000.014849
97487	97654	9.6617E-02	1000.018261
2628	2482	1.9799E-08	1000.019603
20979	21143	4.7356E-09	1000.019857
20839	21343	9.1387E-08	1000.021072

f: Upper state counting number;
i: Lower state counting number;
A_{fi}: Einstein-A coefficient in s^{-1};
$\tilde{\nu}_{fi}$: transition wavenumber in cm^{-1}.

ACKNOWLEDGMENTS

This work was supported by the European Research Council (ERC) under the European Union's Horizon 2020 research and innovation programme through Advance Grant number 883830, and by STFC Projects No. ST/M001334/1, ST/R000476/1 and ST/T001429/1. EN thanks Université Toulouse III - Paul Sabatier for funding for her visit to UCL.

DATA AVAILABILITY

The states, transition and partition function files for the AlCl YNAT line list can be downloaded from www.exomol.com and the CDS data centre cdsarc.u-strasbg.fr. The open access program Duo and is available via github.com/exomol and from zenodo.

During the reviewing process, the YNAT line lists (states, transition, partition function files and Duo inputs) can be downloaded from https://exomol.com/repository/AlCl/YNAT/.

SUPPORTING INFORMATION

Supplementary data are available at MNRAS online comprising the $Al^{35}Cl$ MARVEL (input) transitions and MARVEL (output) energy levels plus a sample Duo input file which specifies potentials, couplings and dipoles as well as the basis sets used for the nuclear motion calculations.

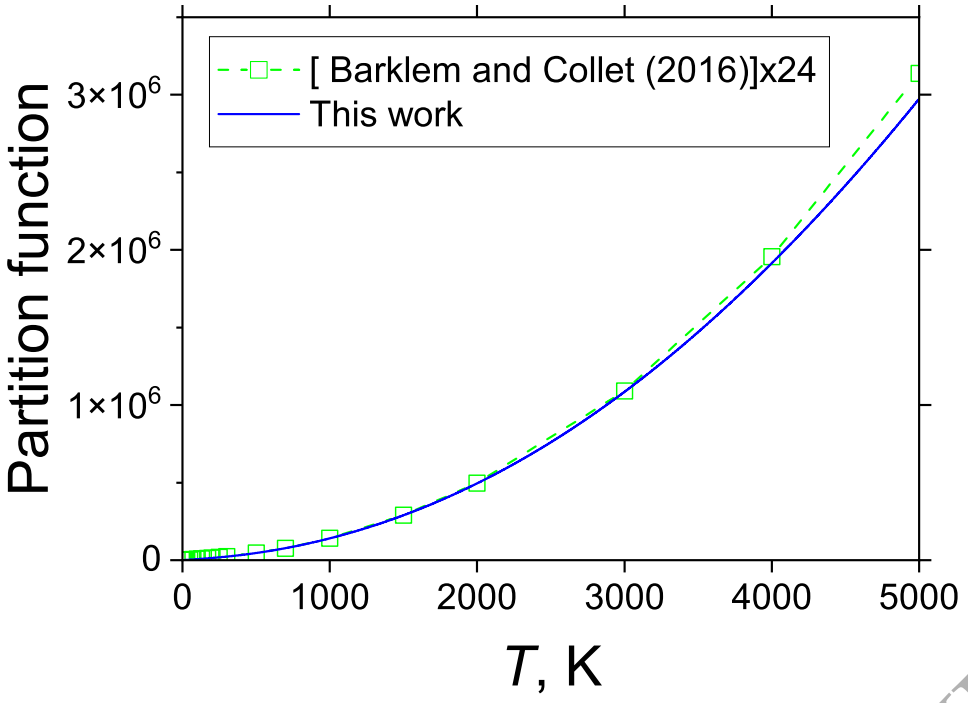

Figure 5. Partition function of $Al^{35}Cl$ compared to that of Barklem & Collet (2016).

REFERENCES

Agundez M., Fonfria J. P., Cernicharo J., Kahane C., Daniel F., Guelin M., 2012, A&A, 543, A48
Barklem P. S., Collet R., 2016, A&A, 588, A96
Cernicharo J., Guelin M., 1987, A&A, 183, L10
Chubb K. L., Min M., Kawashima Y., Helling C., Waldmann I., 2020, A&A, 639, A3
Császár A. G., Furtenbacher T., 2011, J. Mol. Spectrosc., 266, 99
Daniel J. R., Wang C., Rodriguez K., Hemmerling B., Lewis T. N., Bardeen C., Teplukhin A., Kendrick B. K., 2021, Phys. Rev. A, 104, 012801
Danilovich T., et al., 2021, A&A, 655, A80
Decin L., et al., 2017, A&A, 608, A55
European Organization For Nuclear Research OpenAIRE 2013, Zenodo, doi:10.25495/7GXK-RD71, https://www.zenodo.org/
Furtenbacher T., Császár A. G., Tennyson J., 2007, J. Mol. Spectrosc., 245, 115
Gamache R. R., et al., 2017, J. Quant. Spectrosc. Radiat. Transf., 203, 70
Hedderich H. G., Dulick M., Bernath P. F., 1993, J. Chem. Phys., 99, 8363
Hensel K. D., Styger C., JageR W., Merer A. J., Gerry M. C. L., 1993, J. Chem. Phys., 99, 3320
Hoeft J., Torring T., Tiemann E., 1973, Z Naturforsch A, A 28, 1066
Kumar Y., Khanna B. N., Varshney D. C., 1985, Indian J. Pure Appl. Phys., 23, 128
Langhoff S. R., Bauschlicher C. W., Taylor P. R., 1988, J. Chem. Phys., 88, 5715
Lee E. G., Seto J. Y., Hirao T., Bernath P. F., Le Roy R. J., 1999, J. Mol. Spectrosc., 194, 197
Lide D. R., 1965, J. Chem. Phys., 42, 1013
Mahieu E., Dubois I., Bredohl H., 1989a, J. Mol. Spectrosc., 134, 317
Mahieu E., Dubois I., Bredohl H., 1989b, J. Mol. Spectrosc., 138, 264
Medvedev E. S., Meshkov V. V., Stolyarov A. V., Gordon I. E., 2015, J. Chem. Phys., 143, 154301
Pezzella M., Yurchenko S. N., Tennyson J., 2021, Phys. Chem. Chem. Phys., 23, 16390
Pezzella M., Yurchenko S. N., Tennyson J., 2022, MNRAS, 514, 4413
Prajapat L., Jagoda P., Lodi L., Gorman M. N., Yurchenko S. N., Tennyson J., 2017, MNRAS, 472, 3648
Qin Z., Bai T., Liu L., 2021, MNRAS, 508, 2848
Ram R. S., Rai S. B., Rai D. K., Upadhya K. N., 1979, Indian J Phys Proc Indian Assoc Cultiv Sci - Part B, 53, 56
Ram R. S., Rai S. B., Upadhya K. N., Rai D. K., 1982, Physica Scripta, 26, 383
Reddy S. P., Rao P. T., 1957, Can. J. Phys., 35, 912
Saksena M. D., Dixit V. S., Singh M., 1998, J. Mol. Spectrosc., 187, 1
Sharma D., 1951, ApJ, 113, 210
Tennyson J., Yurchenko S. N., 2012, MNRAS, 425, 21
Tennyson J., Hill C., Yurchenko S. N., 2013, in 6^{th} international conference on atomic and molecular data and their applications ICAMDATA-2012. AIP, New York, pp 186–195, doi:10.1063/1.4815853
Tennyson J., et al., 2020, J. Quant. Spectrosc. Radiat. Transf., 255, 107228

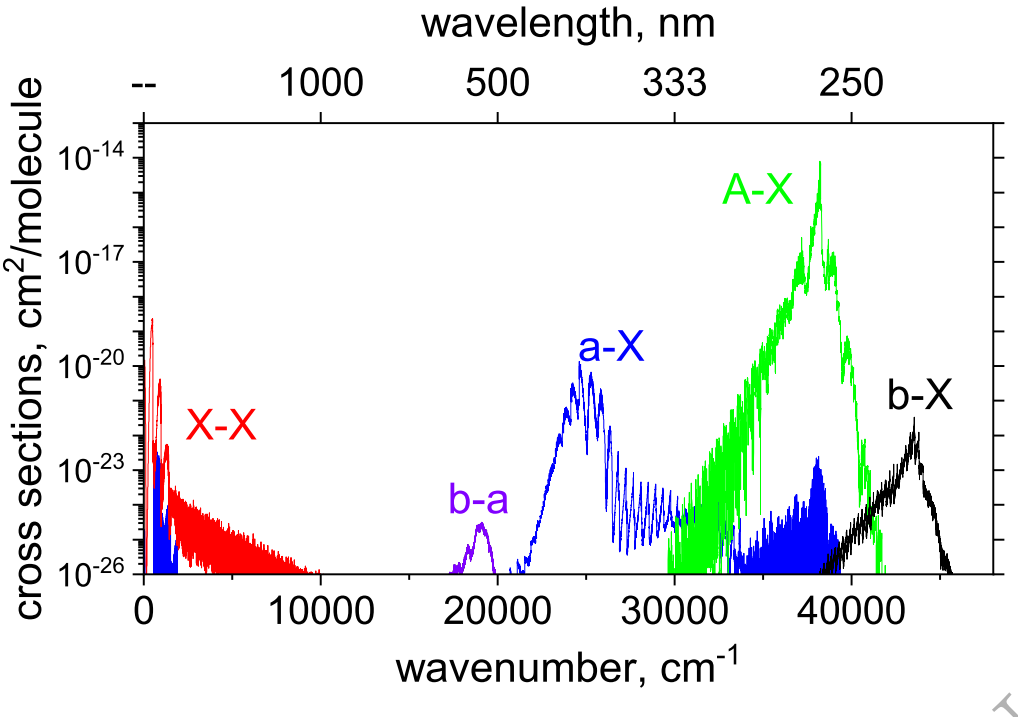

Figure 6. Overview YNAT absorption spectrum of $Al^{35}Cl$ at T = 2000 K using a Gaussian line profile of HWHM = 1 cm^{-1}.

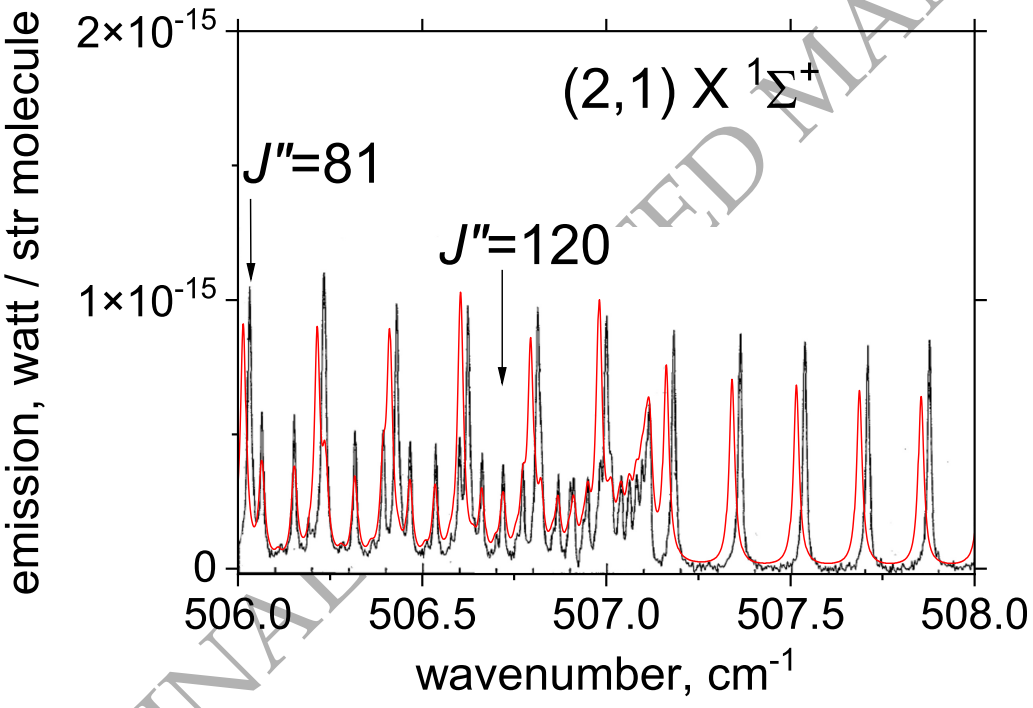

Figure 7. Comparison of the $v' = 2 - v'' = 1$ infrared band of $Al^{35}Cl$ observed in emission by Hedderich et al. (1993) (in black) with the YNAT line list (in red) for an assumed temperature of T = 1400 K and a Lorentzian profile with HWHM = 0.02 cm^{-1}.

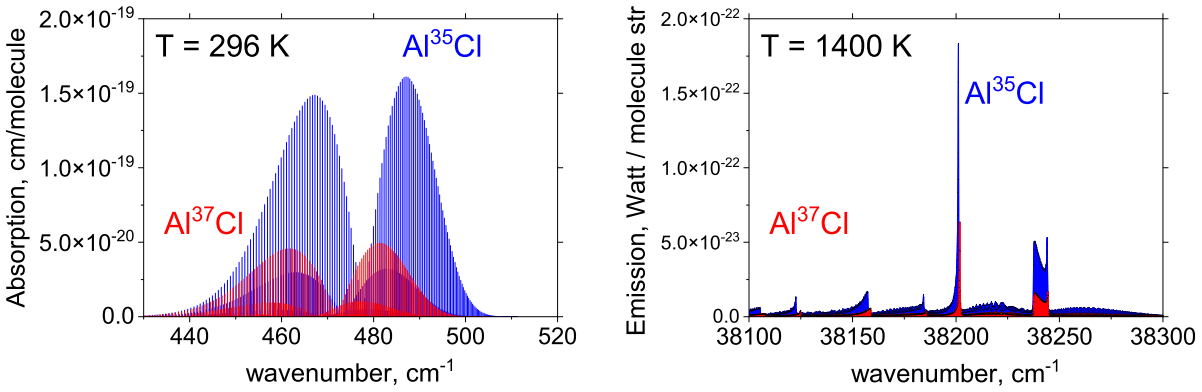

Figure 8. Two bands of two istopologues AlCl.

Tóbiás R., Furtenbacher T., Tennyson J., Császár A. G., 2019, Phys. Chem. Chem. Phys., 21, 3473
Wang Y., Tennyson J., Yurchenko S. N., 2020, Atoms, 8, 7
Welz B., Becker-Ross H., Florek S., Heitmann U., 2006, Electron Excitation Spectra of Diatomic Molecules. John Wiley & Sons, Ltd. pp 158–160, doi:10.1002/3527606513.ch7
Werner H.-J., Knowles P. J., Knizia G., Manby F. R., Schütz M., 2012, WIREs Comput. Mol. Sci., 2, 242
Woitke P., Helling C., Hunter G. H., Millard J. D., Turner G. E., Worters M., Blecic J., Stock J. W., 2018, A&A, 614, A1
Wyse F. C., Gordy W., 1972, J. Chem. Phys., 56, 2130
Xu J.-G., Zhang C.-Y., Zhang Y.-G., 2020, Chinese Phys. B, 29, 033102
Yousefi M., Bernath P. F., 2018, ApJS, 237, 8
Yurchenko S. N., Lodi L., Tennyson J., Stolyarov A. V., 2016, Comput. Phys. Commun., 202, 262
Yurchenko S. N., Sinden F., Lodi L., Hill C., Gorman M. N., Tennyson J., 2018, MNRAS, 473, 5324
Yurchenko S. N., et al., 2022, MNRAS, 510, 903–919